The Cosmic Mach Number: Comparison from Observations, Numerical Simulations and Nonlinear Predictions

by Shankar Agarwal and Hume A. Feldman

2013

Monthly Notices
of the
ROYAL ASTRONOMICAL SOCIETY

MNRAS **432,** 307–317 (2013)
Advance Access publication 2013 April 9

doi:10.1093/mnras/stt464

The cosmic Mach number: comparison from observations, numerical simulations and non-linear predictions

Shankar Agarwal⋆ and Hume A. Feldman⋆

Department of Physics & Astronomy, University of Kansas, Lawrence, KS 66045, USA

Accepted 2013 March 13. Received 2013 February 14; in original form 2012 December 31

ABSTRACT

We calculate the cosmic Mach number M – the ratio of the bulk flow of the velocity field on scale R to the velocity dispersion within regions of scale R. M is effectively a measure of the ratio of large-scale to small-scale power and can be a useful tool to constrain the cosmological parameter space. Using a compilation of existing peculiar velocity surveys, we calculate M and compare it to that estimated from mock catalogues extracted from the Large Suite of Dark Matter Simulations (LasDamas, a Λ cold dark matter cosmology) numerical simulations. We find agreement with expectations for the LasDamas cosmology at $\sim 1.5\sigma$ confidence level. We also show that our Mach estimates for the mocks are not biased by selection function effects. To achieve this, we extract dense and nearly isotropic distributions using Gaussian selection functions with the same width as the characteristic depth of the real surveys, and show that the Mach numbers estimated from the mocks are very similar to the values based on Gaussian profiles of the corresponding widths. We discuss the importance of the survey window functions in estimating their effective depths. We investigate the non-linear matter power spectrum interpolator PKANN as an alternative to numerical simulations, in the study of Mach number.

Key words: galaxies: kinematics and dynamics – galaxies: statistics – cosmology: observations – cosmology: theory – distance scale – large-scale structure of Universe.

1 INTRODUCTION

Ostriker & Suto (1990) introduced a dimensionless statistic of the cosmological structure – the cosmic Mach number, as a way to measure the warmth/coldness of the velocity field on some scale R. Specifically, the Mach number is defined as a ratio

$$M(\boldsymbol{x}_0; R) \equiv \left(\frac{|\boldsymbol{u}(\boldsymbol{x}_0; R)|^2}{\sigma^2(\boldsymbol{x}_0; R)} \right)^{1/2}, \quad (1)$$

where $\boldsymbol{u}(\boldsymbol{x}_0; R)$ is the bulk flow (BF) of a region of size R centred at $\boldsymbol{x}_0$ and $\sigma(\boldsymbol{x}_0; R)$ is the velocity dispersion of the objects within this region. The ensemble average over $\boldsymbol{x}_0$ gives the statistic $M(R)$. Since both $|\boldsymbol{u}(\boldsymbol{x}_0; R)|^2$ and $\sigma^2(\boldsymbol{x}_0; R)$ scale equally by the amplitude of the matter density perturbation, the statistic M is independent (at least in linear approximation) of the normalization of the matter power spectrum.

In linear theory, given the cosmological parameters, M can be readily calculated and compared with its measured value from the peculiar velocity field catalogues. However, comparing theoretical predictions with observations is not straightforward: (i) one has to correct for the small-scale non-linearities in observations as well as take into account the fact that observations represent only a discrete sample of the continuous velocity field. This can be remedied by smoothing the velocity field on a suitable scale r_s ($\sim 5\,h^{-1}$ Mpc, since on larger scales the matter density field is expected to be linear), before estimating the quantities $\boldsymbol{u}(\boldsymbol{x}_0; R)$ and $\sigma(\boldsymbol{x}_0; R)$. However, any residual non-linearity in the observed field can still bias the M estimates; (ii) non-uniform, noisy and sparse sampling of the peculiar velocity field can lead to aliasing of small-scale power on to larger scales. When making comparisons with theory, one has to carefully take into account the selection function and the noise of the real data set. (iii) Peculiar velocity surveys have only line-of-sight velocity information.

Over two decades ago, the statistic M has been investigated in a series of papers: Ostriker & Suto (1990) used linear theory and Gaussian selection function to show that the standard cold dark matter (sCDM) model is inconsistent (predicts M almost twice the observed value) with observations at $\sim$95 per cent confidence level (CL); Suto, Cen & Ostriker (1992), using top-hat and Gaussian selection functions, studied the distribution of M using N-body simulations to rule out the sCDM scenario at 99 per cent CL; Strauss, Cen & Ostriker (1993) took into account the selection function of real surveys and extracted mocks from numerical simulations over a range of cosmologies including sCDM and tilted CDM (scalar spectral index, $n_s \neq 1$) among others to reject the sCDM model at 94 per cent CL.

⋆ E-mail: sagarwal@ku.edu (SA); feldman@ku.edu (HAF)

More recently, Ma, Ostriker & Zhao (2012) explored the potential of using M in distinguishing cosmological models, including modified gravity and massive neutrino cosmologies.

In this paper, (i) we estimate the cosmic Mach number for various galaxy peculiar velocity data sets; (ii) we investigate how likely it is to get these Mach values in a ΛCDM universe. To achieve this, we study the statistical distribution of the expected Mach number by extracting mocks of the real catalogues from numerical simulations of a ΛCDM universe. We show that a ΛCDM universe with 7-yr *Wilkinson Microwave Anisotropy Probe* (*WMAP*) type cosmology is consistent with the Mach observations at $\sim 1.5\sigma$ CL; (iii) we further show that our M estimates for the mocks are not biased by their selection functions. Towards this, we extract dense and nearly isotropic distributions with a Gaussian profile $f(r) \propto \mathrm{e}^{-r^2/2R^2}$ with $R = 10$–$100\ h^{-1}$ Mpc. We show that the Mach numbers estimated from the mocks are very similar to the values based on Gaussian profiles (of similar depth R as the mocks); (iv) we use the non-linear matter power spectrum interpolation scheme PKANN (Agarwal et al. 2012a) to check if we can avoid N-body simulations completely and predict $M(R)$ by only using PKANN's prediction for the non-linear power spectrum. This is crucial because high-resolution hydrodynamic N-body simulations are computationally expensive and extremely time consuming. Exploring parameter space using numerical simulations within reasonable time and computing resources might not be possible. A full use of a statistic like M can only be realized with a prescription for the non-linear matter power spectrum. Matter power spectrum fitting functions based on higher order perturbation theory (e.g. Saito, Takada & Taruya 2008, 2009; Nishimichi et al. 2009) and halo models (HALOFIT; Smith et al. 2003) perform well on large scales ($k \lesssim 0.1\,h\,\mathrm{Mpc}^{-1}$), but their performance degrades on smaller scales. The fitting accuracy from these fits is cosmological model dependent and may be as low as 50 per cent with HALOFIT at $k \sim 1\,h\,\mathrm{Mpc}^{-1}$ (Agarwal et al. 2012a). On the other hand, PKANN has been designed to predict the power spectrum accurate at the sub-per cent level for wavenumbers up to $k \leq 0.9\,h\,\mathrm{Mpc}^{-1}$.

In Section 2, we discuss the cosmic Mach number statistic. In Section 3, we describe the numerical simulations we use to extract mock surveys. In Section 4, we describe the galaxy peculiar velocity surveys (Section 4.1) and the procedure we follow to extract the mock catalogues (Section 4.2). In Section 5, we review the maximum likelihood estimate (hereafter MLE) weighting scheme that is commonly used to analyse peculiar velocity surveys. In Section 6, we show our results for the statistical distribution of the Mach number estimated using various mock catalogues. In Section 7, we test the performance of PKANN – a non-linear matter power spectrum interpolator, in predicting $M(R)$ for the Large Suite of Dark Matter Simulations (LasDamas) cosmology. The Mach number estimates from real surveys are summarized in Section 8. We discuss our results and conclude in Section 9.

2 THE COSMIC MACH NUMBER

Given a peculiar velocity field $\boldsymbol{v}(\boldsymbol{x})$, one can calculate the BF (see Feldman & Watkins 1994 for details), which represents the net streaming motion of a region in some direction relative to the background Hubble expansion. The BF $\boldsymbol{u}(\boldsymbol{x}_0; R)$ of a region of size R centred at $\boldsymbol{x}_0$ can be defined as

$$\boldsymbol{u}(\boldsymbol{x}_0; R) = \int \mathrm{d}\boldsymbol{x}\ \boldsymbol{v}(\boldsymbol{x}) F(|\boldsymbol{x} - \boldsymbol{x}_0|, R), \tag{2}$$

where $F(|\boldsymbol{x} - \boldsymbol{x}_0|, R)$ is the filter used to average the velocity field $\boldsymbol{v}(\boldsymbol{x})$ on a characteristic scale R. Although top-hat and Gaussian filters are the preferred choices, $F(|\boldsymbol{x} - \boldsymbol{x}_0|, R)$ can be designed to mimic the selection function of the real data sets. This is useful when dealing with data sets whose selection function depends strongly on the position in the sky. In Fourier space, equation (2) can be written as

$$\boldsymbol{u}(\boldsymbol{x}_0; R) = \int \mathrm{d}\boldsymbol{k}\ \boldsymbol{v}(\boldsymbol{k}) W(\boldsymbol{k}, R) \mathrm{e}^{-\mathrm{i}\boldsymbol{k}\cdot\boldsymbol{x}_0}, \tag{3}$$

where $\boldsymbol{v}(\boldsymbol{k})$ and $W(\boldsymbol{k}, R)$ are the Fourier transforms of the peculiar velocity field $\boldsymbol{v}(\boldsymbol{x})$ and the filter $F(|\boldsymbol{x} - \boldsymbol{x}_0|, R)$, respectively.

In linear theory of structure formation, at low redshifts, the velocities are related to the matter overdensities via

$$\boldsymbol{v}(\boldsymbol{k}) = \mathrm{i} f H_0 \delta(\boldsymbol{k}) \frac{\boldsymbol{k}}{k^2}, \tag{4}$$

where H_0 is the present-day Hubble parameter in units of km s^{-1} Mpc^{-1}; $\delta(\boldsymbol{k})$ is the Fourier transform of the overdensity field $\delta(\boldsymbol{x})$; the linear growth rate factor f can be approximated as $f = \Omega_\mathrm{m}^{0.55}$ (Linder 2005). Thus, the velocity power spectrum $P_\mathrm{v}(k)$ is proportional to the matter power spectrum $P(k)$ at low redshifts,

$$P_\mathrm{v}(k) = (H_0 f)^2 \frac{P(k)}{k^2}. \tag{5}$$

Using equations (3) and (5), the mean squared bulk value of $\boldsymbol{u}(\boldsymbol{x}_0; R)$ can be shown to be

$$\sigma_\mathrm{v}^2(R) \equiv \left\langle \boldsymbol{u}^2(\boldsymbol{x}_0; R) \right\rangle = \frac{H_0^2 \Omega_\mathrm{m}^{1.1}}{2\pi^2} \int \mathrm{d}k\ P(k) W^2(kR), \tag{6}$$

where the average is taken over all spatial positions $\boldsymbol{x}_0$.

The squared velocity dispersion within a region of size R centred at $\boldsymbol{x}_0$ can be similarly defined as

$$\sigma^2(\boldsymbol{x}_0; R) = \int \mathrm{d}\boldsymbol{x}\ |\boldsymbol{v}(\boldsymbol{x})|^2 F(|\boldsymbol{x} - \boldsymbol{x}_0|, R) - |\boldsymbol{u}(\boldsymbol{x}_0; R)|^2. \tag{7}$$

In Fourier space, the ensemble average of equation (7) over $\boldsymbol{x}_0$ becomes

$$\sigma^2(R) \equiv \left\langle \sigma^2(\boldsymbol{x}_0; R) \right\rangle = \frac{H_0^2 \Omega_\mathrm{m}^{1.1}}{2\pi^2} \int \mathrm{d}k\ P(k) \left(1 - W^2(kR)\right). \tag{8}$$

Using equations (6) and (8), the cosmic Mach number can now be defined as

$$M(R) \equiv \left\langle M^2(\boldsymbol{x}_0; R) \right\rangle^{1/2} = \left(\frac{\sigma_\mathrm{v}^2(R)}{\sigma^2(R)} \right)^{1/2}. \tag{9}$$

As discussed in the literature (Ostriker & Suto 1990; Suto et al. 1992; Strauss et al. 1993), the cosmic Mach number is essentially a measure of the shape of the matter power spectrum (Watkins & Feldman 2007). The rms BF $\sigma_\mathrm{v}(R)$ gets most of its contribution from scales larger than R, while the velocity dispersion $\sigma(R)$ is a measure of the magnitude of velocities on scales smaller than R and gets most contribution from small scales (for more detailed analyses of velocity dispersion, see Bahcall, Gramann & Cen 1994; Bahcall & Oh 1996; Watkins 1997). Furthermore, the statistic M is expected to be independent of the matter power spectrum normalization – at least on large scales, where the perturbations are still well described by linear theory and affect both $\sigma_\mathrm{v}^2(R)$ and $\sigma^2(R)$ equally. M can be a powerful tool to test not only the ΛCDM scenario, but also a wide range of cosmologies including models with massive neutrinos. Massive neutrinos suppress the matter power spectrum in a scale-dependent way, thereby altering the velocity dispersion much more prominently than the BF. The Mach number M provides an

Table 1. The cosmological parameters and the design specifications of the LD-*Carmen* simulations.

Cosmological parameters	LD-*Carmen*
Matter density, Ω_m	0.25
Cosmological constant density, Ω_Λ	0.75
Baryon density, Ω_b	0.04
Hubble parameter, h (100 km s^{-1} Mpc^{-1})	0.7
Amplitude of matter density fluctuations, σ_8	0.8
Primordial scalar spectral index, n_s	1.0
Simulation design parameters	
Simulation box size on a side (h^{-1} Mpc)	1000
Number of CDM particles	1120^3
Initial redshift, z	49
Particle mass, m_p (10^{10} h^{-1} $M_\odot$)	4.938
Gravitational force softening length, f_ϵ (h^{-1} kpc)	53

easy-to-interpret technique to distinguish between various cosmological models.

In previous work (Watkins, Feldman & Hudson 2009; Feldman, Watkins & Hudson 2010; Agarwal, Feldman & Watkins 2012b), we have dealt with peculiar velocity surveys differently. We developed the 'minimum variance' (hereafter MV) formalism to make a clean estimate of the bulk, shear and the octupole moments of the velocity field as a function of scale using the available peculiar velocity data. Higher moments get contribution from progressively smaller scales. In this paper, instead of isolating the higher moments (shear, octupole, etc.), we simply estimate the velocity dispersion $\sigma(R)$ that gets contribution from all scales smaller than R. In general, the MLE scheme we employ here attempts to minimize the error given a particular survey. The downside of the MLE formalism is the difficulty to directly compare results from different surveys. Since each survey samples the volume differently and although the large-scale signal is similar across surveys, the small-scale noise is unique. This leads to complicated biases or aliasing that are survey dependent (see Watkins & Feldman 1995; Hudson et al. 2000). The MV formalism corrects for small-scale aliasing by using a minimization scheme that treats the volume of the surveys rather than the particular way the survey samples the volume, thus eliminating aliasing and allowing for direct comparison between surveys.

3 *N*-BODY SIMULATIONS

In order to study the statistical distribution of the cosmic Mach number, we extract mock surveys from the 41 numerical realizations of a ΛCDM universe. The *N*-body simulation we use in our analysis is LasDamas (hereafter LD; McBride et al. 2009; McBride et al. 2011, in preparation[1]). The LD simulation is a suite of 41 independent realizations of dark matter *N*-body simulations named *Carmen* and has information at redshift $z = 0.13$. Using the Ntropy framework (Gardner, Connolly & McBride 2007), bound groups of dark matter particles (haloes) are identified with a parallel friends-of-friends (FOF) code (Davis et al. 1985). The cosmological parameters and the design specifications of the LD-*Carmen* are listed in Table 1.

We extract 100 mock catalogues from each of the 41 LD-*Carmen* boxes, for a total of 4100 mocks. The mocks are randomly centred inside the boxes. They are extracted to mimic the radial distribution of the real catalogues (described in Section 4.1), as closely as possible.

[1] http://lss.phy.vanderbilt.edu/lasdamas

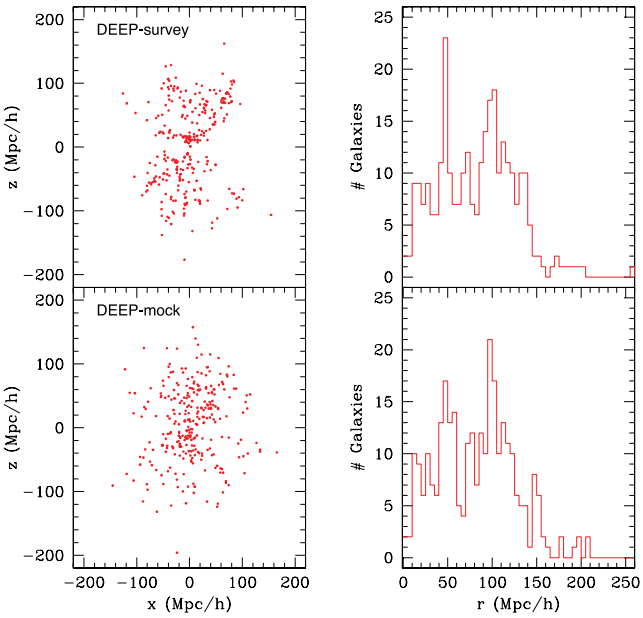

Figure 1. Top row: DEEP catalogue (left) and its radial distribution (right). Bottom row: DEEP mock catalogue (left) and its radial distribution (right).

4 PECULIAR VELOCITY CATALOGUES

4.1 Real catalogues

We use a compilation of five galaxy peculiar velocity surveys to study the Mach statistic. This compilation, which we label 'DEEP', includes 103 Type Ia supernovae (SNIa; Tonry et al. 2003), 70 spiral galaxy clusters (SC) Tully–Fisher (TF) clusters (Giovanelli et al. 1998; Dale et al. 1999), 56 Streaming Motions of Abell Clusters (SMAC) Fundamental Plane (FP) clusters (Hudson et al. 1999, 2004), 50 early-type far galaxies (EFAR) FP clusters (Colless et al. 2001) and 15 TF clusters (Willick 1999). In all, the DEEP catalogue consists of 294 data points. In Fig. 1, top row, we show the DEEP catalogue (left-hand panel) and its radial distribution (right-hand panel). The bottom row shows a typical mock extracted from the LD simulations. The procedure to extract mocks is described in Section 4.2.

4.2 Mock catalogues

Inside the *N*-body simulation box, we first select a point at random. Next, we extract a mock realization of the real catalogue by imposing the constraint that the mock should have a similar radial distribution to the real catalogue. We do not constrain the mocks to have the same angular distribution as the real catalogue for two reasons: (i) the LD simulation boxes are not dense enough to give us mocks that are exact replicas of the real catalogue and (ii) the objects in a real survey are typically weighted depending only on their velocity errors. Consequently, even though the real catalogue and its mocks have similar radial profiles, their angular distributions differ considerably, with the mocks having a relatively featureless angular distribution. To make the mocks more realistic, we impose a 10° latitude zone-of-avoidance cut.

Using the angular position $\{\hat{r}_x, \hat{r}_y, \hat{r}_z\}$, the true radial distance d_s from the mock centre and the peculiar velocity vector $\boldsymbol{v}$, we calculate the true line-of-sight peculiar velocity v_s and the redshift $cz = d_s + v_s$ for each mock galaxy (in km s^{-1}). We then perturb the true radial distance d_s of the mock galaxy with a velocity error drawn from a Gaussian distribution of width equal to the corresponding real galaxy's velocity error, e. Thus, $d_p = d_s + \delta_d$, where d_p is the perturbed radial distance of the mock galaxy (in km s^{-1}) and δ_d is the velocity error drawn from a Gaussian of width e. The mock galaxy's measured line-of-sight peculiar velocity v_p is then assigned to be $v_p = cz - d_p$, where cz is the redshift we found above. This procedure ensures that the weights we assign to the mock galaxies are similar to the weights of the real galaxies. In Fig. 1, we show the angular (left-hand panels) and radial (right-hand panels) distribution of galaxies in the DEEP catalogue (top) and its mock (bottom).

5 THE MLE METHOD

One of the most common weighting scheme used in the analysis of the BF is the MLE method, obtained from a maximum likelihood analysis introduced by Kaiser (1988). The motion of galaxies is modelled as being due to a streaming flow with Gaussian distributed measurement uncertainties. Given a peculiar velocity survey, the MLE of its BF is obtained from the likelihood function

$$L[u_i|\{S_n, \sigma_n, \sigma_*\}] = \prod_n \frac{1}{\sqrt{\sigma_n^2 + \sigma_*^2}} \exp\left(\frac{-\frac{1}{2}(S_n - \hat{r}_{n,i}u_i)^2}{\sigma_n^2 + \sigma_*^2}\right), \tag{10}$$

where $\hat{\boldsymbol{r}}_n$ is the unit position vector of the nth galaxy, σ_n is the measurement uncertainty of the nth galaxy and σ_* is the 1D velocity dispersion accounting for smaller scale motions. The three components of the BF u_i can be written as a weighted sum of the measured radial peculiar velocities of a survey

$$u_i = \sum_n w_{i,n} S_n, \tag{11}$$

where S_n is the radial peculiar velocity of the nth galaxy of a survey and $w_{i,n}$ is the weight assigned to this velocity in the calculation of u_i. Throughout this paper, subscripts i, j and k run over the three spatial components of the BF, while subscripts m and n run over the galaxies. Maximizing the likelihood given by equation (10) gives the three components of the BF u_i with the MLE weights

$$w_{i,n} = \sum_{j=1}^{3} A_{ij}^{-1} \frac{\hat{r}_{n,j}}{\sigma_n^2 + \sigma_*^2}, \tag{12}$$

where

$$A_{ij} = \sum_n \frac{\hat{r}_{n,i}\hat{r}_{n,j}}{\sigma_n^2 + \sigma_*^2}. \tag{13}$$

The 1D velocity dispersion σ_* is $1/\sqrt{3}$ of the 3D velocity dispersion (see equation 8) which we aim to ultimately measure. Since the weights $w_{i,n}$ (and u_i) are themselves a function of σ_*, we converge on to the MLE for σ_* iteratively. See Strauss et al. (1993) for a discussion on how to estimate the best-fitting u_i and σ_*.

The effective depth of a survey can be roughly estimated by a weighted sum $\sum w_n r_n / \sum w_n$ of the radial distances r_n of the survey objects, where $w_n = 1/(\sigma_n^2 + \sigma_*^2)$. This weighting scheme has been used by Ma et al. (2012) in their analyses of peculiar velocity data sets. A drawback of using weights $w_n = 1/(\sigma_n^2 + \sigma_*^2)$ in estimating the depth of a survey is that while the weights w_n take into account the measurement errors σ_n, they do not make any corrections for the survey geometry. A better estimate of the effective depth can be made by looking at the survey window functions W_{ij}^2. The window function gives an idea of the scales that contribute to the BF estimates. Ideally, the window function should fall quickly to zero for scales smaller than that being studied. This ensures that the BF estimates are minimally biased from small-scale non-linearities.

Armed with the MLE weights $w_{i,n}$ from equation (12), the angle-averaged tensor window function $W_{ij}^2(k)$ [equivalent to $W^2(kR)$ of equation 6] can be constructed (for details, see Feldman et al. 2010) as

$$W_{ij}^2(k) = \sum_{m,n} w_{i,m} w_{j,n} \int \frac{\mathrm{d}^2\hat{k}}{4\pi} (\hat{\boldsymbol{r}}_m \cdot \hat{\boldsymbol{k}})(\hat{\boldsymbol{r}}_n \cdot \hat{\boldsymbol{k}}) \times \exp(\mathrm{i}k\, \hat{\boldsymbol{k}} \cdot (\boldsymbol{r}_m - \boldsymbol{r}_n)). \tag{14}$$

The diagonal elements W_{ii}^2 are the window functions of the BF components u_i. The window function gives an idea of the scales that contribute to the BF estimates. Ideally, the window function should fall quickly to zero for scales smaller than that being studied. This ensures that the BF estimates are minimally biased from small-scale non-linearities. See the MLE (Sarkar, Feldman & Watkins 2007) and MV (Watkins et al. 2009) window functions of the BF components for a range of surveys.

Having constructed the survey window functions W_{ii}^2, the effective depth of the survey can be defined to be the one for which W_{ii}^2 is a close match to the window function for an idealized survey. In order to construct the ideal window functions, we first imagine an idealized survey containing radial velocities that well sample the velocity field in a region. This survey consists of a large number of objects, all with zero measurement uncertainty. The radial distribution of this idealized survey is taken to have a Gaussian profile of the form $f(r) \propto \mathrm{e}^{-r^2/2R^2}$, where R gives a measure of the depth of the survey. This idealized survey has easily interpretable BF components that are not affected by small-scale aliasing and that reflect the motion of a well-defined volume.

The MLE weights of an ideal, isotropic survey consisting of N' exact radial velocities $v_{n'}$ measured at randomly selected positions $\boldsymbol{r}'_{n'}$ are

$$w'_{i,n'} = \sum_{j=1}^{3} A_{ij}^{-1} \frac{\hat{r}'_{n',j}}{N'}, \tag{15}$$

where

$$A_{ij} = \sum_{n'=1}^{N'} \frac{\hat{r}'_{n',i}\hat{r}'_{n',j}}{N'}. \tag{16}$$

Similar to equation (14), the window functions ${}^{I}W_{ij}^2$ for an idealized survey of scale R can be constructed as

$${}^{I}W_{ij}^2(k;R) = \sum_{m,n} w'_{i,m'} w'_{j,n'} \int \frac{\mathrm{d}^2\hat{k}}{4\pi} (\hat{\boldsymbol{r}}'_m \cdot \hat{\boldsymbol{k}})(\hat{\boldsymbol{r}}'_n \cdot \hat{\boldsymbol{k}}) \times \exp(\mathrm{i}k\, \hat{\boldsymbol{k}} \cdot (\boldsymbol{r}'_m - \boldsymbol{r}'_n)). \tag{17}$$

In Fig. 2, left-hand panel, we show the diagonal window functions W_{ii}^2 (see equation 14) of the BF components calculated using MLE weights (see equation 12) for the DEEP catalogue. The x, y, z components are dot–dashed, short-dashed and long-dashed lines, respectively. Also shown are the ideal window functions ${}^{I}W_{ij}^2$

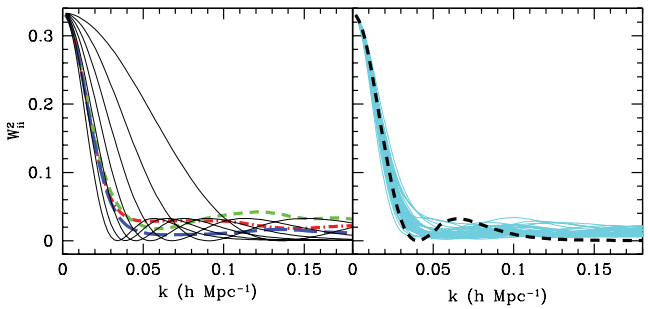

Figure 2. Left-hand panel: the window functions W_{ii}^2 of the BF components calculated using MLE weights for the DEEP catalogue. The x, y, z components are dot–dashed, short-dashed and long-dashed lines, respectively. The solid lines denote the ideal window functions ${}^{I}W_{ij}^2$ for scales $R = 10{-}40\ h^{-1}$ Mpc (in 5 h^{-1} Mpc increments), the window functions being narrower for larger scales. Right-hand panel: the window functions for a subset of the 4100 DEEP mocks (solid lines). The characteristic depth of the DEEP catalogue and its mocks is $R = 34\ h^{-1}$ Mpc (dashed line).

(see equation 17) for scales $R = 10$–$40\ h^{-1}$ Mpc (in 5 h^{-1} Mpc increments), the window functions being narrower for larger scales. To estimate the effective depth R of the DEEP catalogue, we perform a χ^2 minimization of the difference between the DEEP and the ideal window functions for a range of scales $R = 5{-}100\ h^{-1}$ Mpc to obtain the best-fitting $R = 34\ h^{-1}$ Mpc. We note that the weighted sum $\sum w_n r_n / \sum w_n$ gives the DEEP catalogue a depth of 59 h^{-1} Mpc, an overestimation by nearly 70 per cent. Estimating the survey depth correctly is crucial when it comes to comparing the survey BF with theoretical predictions. One might have a high-quality survey but a poorly estimated depth which can introduce substantial errors when comparing with theory. Throughout this paper, we define the characteristic depth R of a survey as the one that minimizes the χ^2 statistic between the survey and the ideal window functions. The right-hand panel of Fig. 2 shows the window functions for a subset of the 4100 DEEP mocks (solid lines) extracted from the LD-*Carmen* simulations. The fact that the mock window functions are nearly centred on the $R = 34\ h^{-1}$ Mpc ideal window shows that our procedure for mock extraction works well.

6 COSMIC MACH NUMBER STATISTICS

6.1 Mach statistics for DEEP mocks

Using the MLE weighting scheme (Section 5), we estimated the BF moments $\{u_x, u_y, u_z\}$, the velocity dispersion σ and the cosmic Mach number M for each of the 4100 DEEP mock realizations. In Fig. 3, we show the probability distribution for the 4100 DEEP mocks: BF u (left-hand panel), dispersion σ (middle panel) and the cosmic Mach number M (right-hand panel). We found the rms BF to be $\sigma_v = 222 \pm 86$ km s^{-1} with a velocity dispersion of $\sigma = 511 \pm 98$ km s^{-1}. Together this implies $M = 0.43 \pm 0.17$ at 1σ CL. Since the DEEP mocks have a characteristic depth of $R = 34\ h^{-1}$ Mpc, we can say that for the LD cosmology, the expected Mach number on scales of $R = 34\ h^{-1}$ Mpc is $M = 0.43 \pm 0.17$.

6.2 Mach statistics for Gaussian realizations

In order to find the expected Mach number as a function of scale R for the LD cosmology, we went to the same central points for each of the 4100 DEEP mocks and computed the weighted average of the velocities of all the galaxies in the simulation box, the weighting function being $e^{-r^2/2R^2}$. We repeated this for a range of scales $R = 10$–$100\ h^{-1}$ Mpc in increments of 5 h^{-1} Mpc. We summarize the expected values for the bulk, dispersion and Mach number for scales $R = 10$–$100\ h^{-1}$ Mpc in Table 2. In Fig. 4, we show the expected values for the bulk, dispersion and Mach number (dashed line) together with their 1σ CL intervals. The corresponding values for the 4100 DEEP mocks are shown by a solid circle at the characteristic scale $R = 34\ h^{-1}$ Mpc.

The expected bulk ($\sigma_v = 234 \pm 94$ km s^{-1}), dispersion ($\sigma = 517 \pm 56$ km s^{-1}) and Mach number ($\sigma = 0.44 \pm 17$) for the Gaussian window with $R = 35\ h^{-1}$ Mpc are in good agreement with the corresponding values for the DEEP mocks. This shows that the DEEP catalogue probes scales up to $R \approx 35\ h^{-1}$ Mpc, and not $R = 59\ h^{-1}$ Mpc as one would have inferred from $\sum w_n r_n / \sum w_n$ using the weights $w_n = 1/(\sigma_n^2 + \sigma_*^2)$.

Linear theory predictions for the LD cosmology are shown by the solid lines in Fig. 4. The onset of non-linear growth in structure formation at low redshifts boosts the velocity dispersion, causing linear theory to overpredict the Mach values.

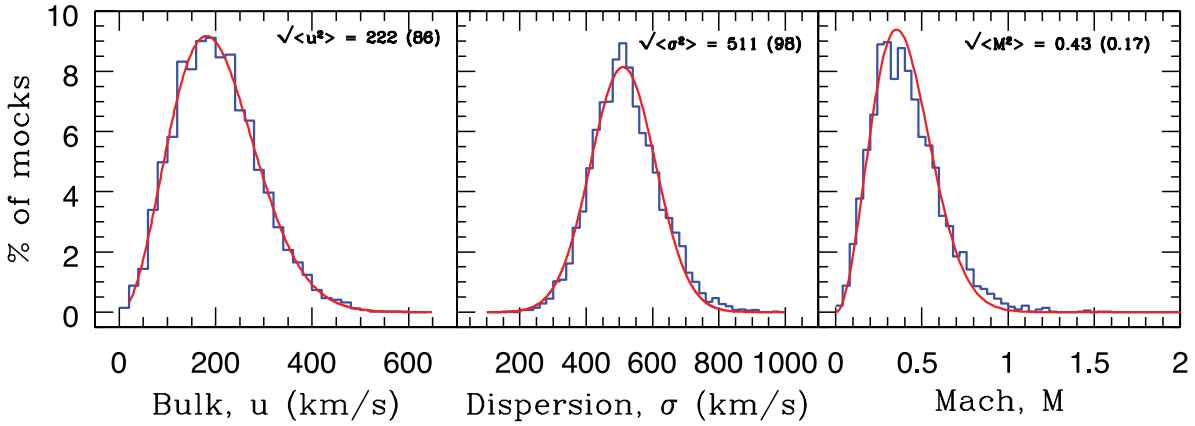

Figure 3. Histograms showing the normalized probability distribution for the 4100 DEEP mocks: BF u (left-hand panel), dispersion σ (middle panel) and the cosmic Mach number M (right-hand panel). We also superimpose the best-fitting Maxwellian (for bulk and Mach) and Gaussian (for dispersion) distributions with the same widths as the corresponding histograms. The rms values and the 1σ CL intervals are mentioned within each panel. The DEEP mocks were extracted from the LD simulations (for the LD parameters, see Table 1).

Table 2. The rms values of the BF (column 2), velocity dispersion (column 3) and cosmic Mach number (column 4) together with their 1σ CL intervals for Gaussian windows with width R (column 1). These values are calculated from the LD simulations (for the LD parameters, see Table 1) using $e^{-r^2/2R^2}$ as the galaxy weighting function, and correspond to the dashed lines in Fig. 4. Linear theory predictions (columns 5–7) correspond to the solid lines in Fig. 4.

	LD simulations			Linear theory		
R	$\sqrt{\langle u^2\rangle}$	$\sqrt{\langle \sigma^2\rangle}$	$\sqrt{\langle M^2\rangle}$	$\sqrt{\langle u^2\rangle}$	$\sqrt{\langle \sigma^2\rangle}$	$\sqrt{\langle M^2\rangle}$
(h^{-1} Mpc)	(km s^{-1})	(km s^{-1})		(km s^{-1})	(km s^{-1})	
10	341 ± 133	379 ± 108	0.85 ± 0.33	369	299	1.23
15	308 ± 120	433 ± 89	0.68 ± 0.27	332	338	0.98
20	286 ± 111	464 ± 76	0.59 ± 0.23	303	365	0.83
25	267 ± 104	487 ± 68	0.53 ± 0.21	280	383	0.73
30	248 ± 96	504 ± 62	0.48 ± 0.19	259	397	0.65
35	234 ± 91	517 ± 56	0.44 ± 0.17	242	408	0.59
40	218 ± 85	526 ± 50	0.41 ± 0.16	227	417	0.54
45	204 ± 79	535 ± 47	0.38 ± 0.15	213	424	0.50
50	194 ± 75	541 ± 43	0.35 ± 0.14	202	430	0.47
55	182 ± 71	547 ± 40	0.33 ± 0.13	191	435	0.44
60	173 ± 67	551 ± 37	0.31 ± 0.12	181	439	0.41
65	163 ± 63	556 ± 35	0.29 ± 0.11	172	442	0.39
70	154 ± 60	560 ± 33	0.27 ± 0.11	164	445	0.37
75	145 ± 57	562 ± 31	0.26 ± 0.10	156	448	0.35
80	137 ± 53	565 ± 29	0.24 ± 0.09	150	450	0.33
85	130 ± 51	567 ± 27	0.23 ± 0.09	143	452	0.32
90	125 ± 48	569 ± 26	0.22 ± 0.08	138	454	0.30
95	118 ± 46	571 ± 25	0.21 ± 0.08	132	456	0.29
100	113 ± 44	572 ± 23	0.20 ± 0.07	127	457	0.28

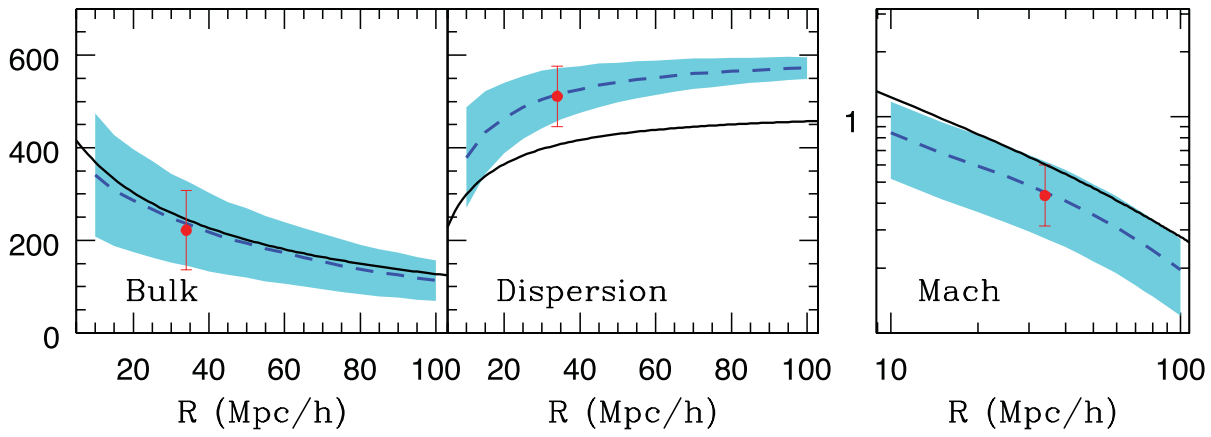

Figure 4. The rms values of the BF (left-hand panel), dispersion (middle panel) and the cosmic Mach number (right-hand panel) are plotted as a function of scale R. In each panel, the dashed line corresponds to measurements from the Gaussian realizations with the shaded region being the 1σ CL interval. The solid circle at $R = 34\ h^{-1}$ Mpc is the result for the DEEP mocks. The error bar is the statistical variance of the mean calculated from the 4100 DEEP mocks. The LD simulations are used to extract the Gaussian and the DEEP mocks. Linear theory predictions are shown by the solid line. The non-linear contributions to the dispersion are clearly seen in both the middle and right-hand panels.

The probability distributions for u, σ and M from the Gaussian realizations in the LD simulations are plotted in Fig. 5 for a range of Gaussian widths R. For clarity, we only show scales $R = 15, 35, 55, 75$ and $95\ h^{-1}$ Mpc.

As expected, the rms BF (dispersion) is a declining (increasing) function of scale R (see Figs 4 and 5). This can be readily understood from the ideal window functions in Fig. 2. Larger scales have narrower window functions in Fourier space. Only small-scale modes ($k \propto 1/R$) contribute to the rms BF integral in equation (6), resulting in smaller BF on larger scales. The dispersion integral (see equation 8) gets most of its contribution from higher k-values ($k > 1/R$) and gradually increases with narrower windows. Similar histogram trends were found by Suto et al. (1992) from numerical simulations of a CDM universe.

6.3 Mach statistics for other mocks

In the following we extend our analysis to include various different peculiar velocity surveys, specifically to show that our results are not dependent on any radial or angular distributions, nor any distinct morphological types. We compared the Gaussian realizations with mocks (4100 each) created to emulate the radial selection function of the surface brightness fluctuations (SBF; Tonry et al. 2001), early-type nearby galaxies (ENEAR; da Costa et al. 2000; Bernardi et al.

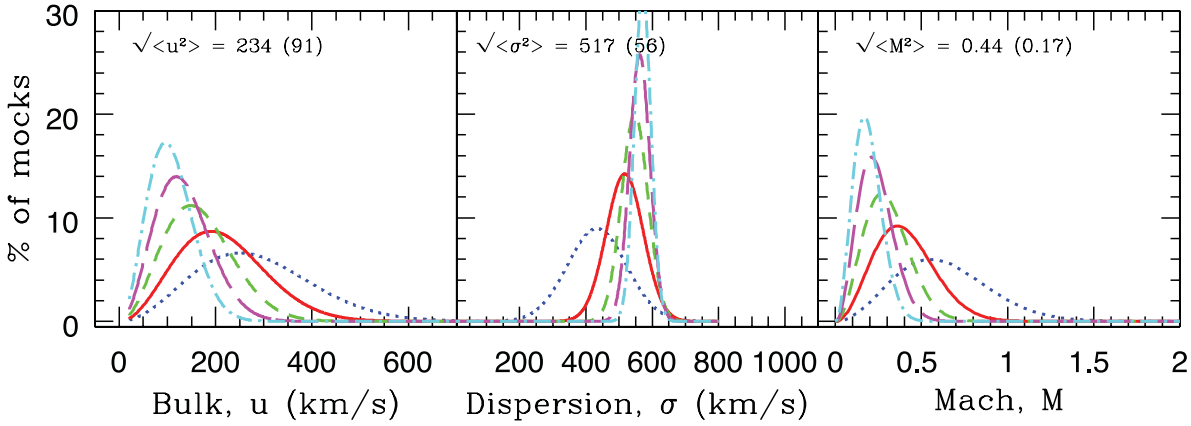

Figure 5. The same as Fig. 3, but for the Gaussian window with $R = 15\ h^{-1}$ Mpc (dotted), $R = 35\ h^{-1}$ Mpc (solid), $R = 55\ h^{-1}$ Mpc (short-dashed), $R = 75\ h^{-1}$ Mpc (long-dashed) and $R = 95\ h^{-1}$ Mpc (dot–dashed). For clarity, instead of the histograms, only the best-fitting Maxellian/Gaussian distributions with the same widths as the corresponding histograms are shown. The rms values and the 1σ CL intervals for $R = 35\ h^{-1}$ Mpc are listed within each panel and are in good agreement with the corresponding values for the DEEP mocks (shown in Fig. 3). Table 2 summarizes the results for Gaussian widths $R = 10-100\ h^{-1}$ Mpc.

2002; Wegner et al. 2003), spiral field *I*-band (SFI++), SNIa and SC peculiar velocity surveys. Note that the SC and SNIa surveys are also part of our DEEP compilation. The SFI++ catalogue (Masters et al. 2006; Springob et al. 2007, 2009) is the densest and most complete peculiar velocity survey of field spirals to date. We use data from Springob et al. (2009). The sample consists of 2720 TF field galaxies (SFI++f) and 736 groups (SFI++g).

In Fig. 6, left-hand panels, we show the window functions W_{ii}^2 of the BF components for the SBF, ENEAR, SFI++g, SNIa, SFI++f, DEEP and SC catalogues (top to bottom row, respectively). The right-hand panels show the window functions for a subset of the corresponding mocks. Through a χ^2 minimization of the difference between the ideal window functions (solid lines in Fig. 6, left-hand panels) and those of the real catalogues, we obtain the characteristic depths of the SBF, ENEAR, SFI++g, SNIa, SFI++f, DEEP and SC catalogues to be $R = 10, 19, 20, 23, 30, 34$ and $40\ h^{-1}$ Mpc, respectively. The ideal window functions for these depths are shown in the right-hand panels (dashed lines, top to bottom row).

In Table 3, we summarize the results for the various surveys (column 1), where the surveys are listed in order of increasing characteristic depth *R* (column 2) (based on the window functions in Fig. 6, as described in Section 5). The error-weighted depths

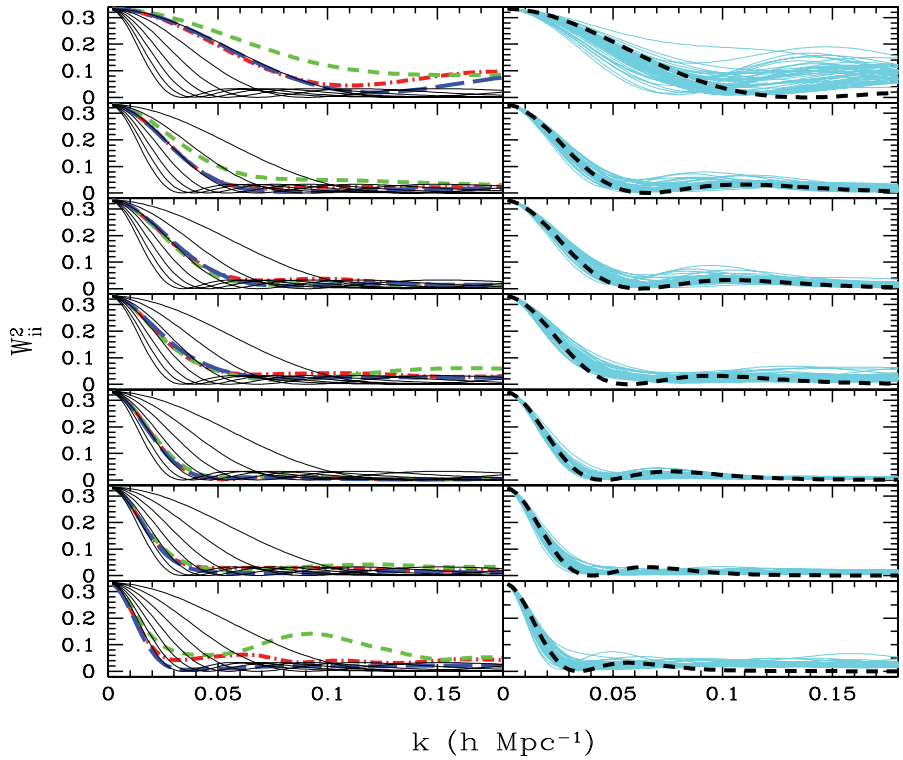

Figure 6. Similar to Fig. 2, for the SBF, ENEAR, SFI++g, SNIa, SFI++f, DEEP and SC catalogues (top to bottom row, respectively).

Table 3. Peculiar velocity statistics for various surveys (column 1). For each survey, 4100 mocks were extracted from the LD cosmology (for the LD parameters, see Table 1). The characteristic depth R (column 2) of the mock catalogues is estimated from the effective width of their window functions shown in Fig. 6. For reference, the error-weighted depth $\sum w_n r_n / \sum w_n$ where $w_n = 1/(\sigma_n^2 + \sigma_*^2)$, is listed in the third column. The rms values of the BF (column 4), velocity dispersion (column 5) and cosmic Mach number (column 6) together with their 1σ CL intervals. Columns 7−9 correspond to the real surveys with the quoted errors calculated using the radial distance uncertainties.

			Mocks			Real		
Survey	R	$\frac{\sum w_n r_n}{\sum w_n}$	$\sqrt{\langle u^2 \rangle}$	$\sqrt{\langle \sigma^2 \rangle}$	$\sqrt{\langle M^2 \rangle}$	u	σ	M
	(h^{-1} Mpc)	(h^{-1} Mpc)	(km s^{-1})	(km s^{-1})		(km s^{-1})	(km s^{-1})	
SBF	10	19	322 ± 125	415 ± 100	0.74 ± 0.29	354 ± 66	428 ± 32	0.83 ± 0.15
ENEAR	19	34	262 ± 102	490 ± 104	0.53 ± 0.21	292 ± 46	528 ± 24	0.55 ± 0.09
SFI++g	20	35	280 ± 101	473 ± 66	0.59 ± 0.18	221 ± 57	436 ± 27	0.29 ± 0.08
SNIa	23	42	275 ± 107	465 ± 73	0.58 ± 0.21	430 ± 87	478 ± 47	0.90 ± 0.18
SFI++f	30	52	240 ± 86	510 ± 81	0.47 ± 0.15	320 ± 44	503 ± 22	0.42 ± 0.06
DEEP	34	59	222 ± 86	511 ± 65	0.43 ± 0.17	312 ± 61	446 ± 27	0.70 ± 0.14
SC	40	75	227 ± 88	485 ± 43	0.47 ± 0.15	116 ± 123	520 ± 74	0.22 ± 0.23

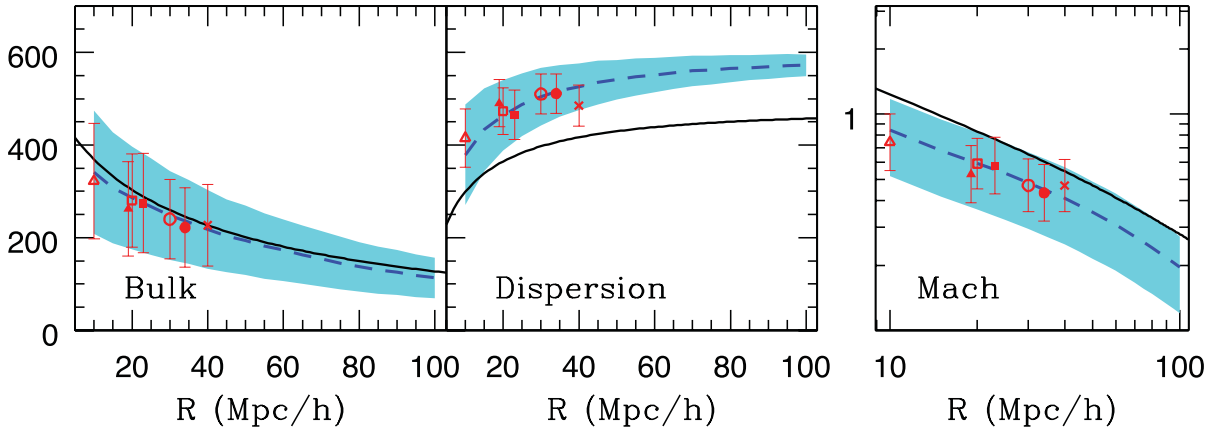

Figure 7. Similar to Fig. 4, including results for the SBF (open triangle), ENEAR (solid triangle), SFI++g (open square), SNIa (solid square), SFI++f (open circle), DEEP (solid circle) and SC (cross) mocks. The DEEP compilation includes the SC, SNIa, SMAC, EFAR and Willick surveys.

$\sum w_n r_n / \sum w_n$, where $w_n = 1/(\sigma_n^2 + \sigma_*^2)$, are listed in column 3 and are typically ∼75 per cent larger than R. For the mock surveys, the expected values for the bulk, dispersion and Mach number and their 1σ CL intervals are summarized in columns 4−6. Columns 7−9 are computed using the real surveys. The quoted errors are calculated using the measurement uncertainties σ_n of the nth galaxy of a survey. Comparing columns 6 and 9, the Mach estimates for all catalogues agree at $\sim 1.5\sigma$ CL for the LD cosmology. Also, comparing the bulk, dispersion and Mach numbers for Gaussian mocks (Table 2, columns 2–4) with the corresponding numbers for the survey mocks (Table 3, columns 4–6), we see that our estimates for the effective survey depth R are correct to within $\pm 5\ h^{-1}$ Mpc.

Similar to Fig. 4, we show results for the SBF, ENEAR, SFI++g, SNIa, SFI++f and SC mocks in Fig. 7. Except for the SBF and SC catalogues, the results for the other catalogues are a close match to their Gaussian counterparts. Our SBF mocks are deeper than the real SBF survey because the LD simulations are not dense enough to extract mocks with depths less than $\sim R = 12\ h^{-1}$ Mpc. This explains why the SBF window functions for the mocks (see Fig. 6, first row, right-hand panel) are narrower than the one for the SBF's depth of $R = 10\ h^{-1}$ Mpc. Narrower window functions decrease (increase) our BF (dispersion) estimates for the SBF mocks. For the SC mocks, the BF (dispersion) gets excess (suppressed) contribution from smaller scales due to the extended tails of the window functions (see Fig. 6, row 7). The SC catalogue, with only 70 clusters, does not have a good sky coverage. The DEEP compilation, however, has a much better sky coverage, and the results (see Fig. 7, solid circle) match those from $R \approx 35\ h^{-1}$ Mpc Gaussian mocks. We have included the results for the SBF and SC catalogues to specifically show that if the selection function of the real survey is not properly modelled, the predictions (in our case, based on the Gaussian selection function) can be misleading.

For reasonably dense and well-sampled velocity surveys, like DEEP, SFI++f and SFI++g, a close match between the mock and the Gaussian results shows that the Mach analysis for such catalogues is not overly sensitive to the selection functions of the individual mocks. As such, one can skip the step of extracting mock realizations of the observations from N-body simulations, and simply use Mach predictions based on the Gaussian selection function $\mathrm{e}^{-r^2/2R^2}$ with R set to the characteristic depth of the survey being studied.

7 MOVING BEYOND *N-BODY* SIMULATIONS: MACH PREDICTIONS USING PKANN

In Section 6, we showed that for velocity surveys with low contamination from small scales, reasonably accurate predictions for the Mach number can be made by extracting mocks having a Gaussian radial profile $\mathrm{e}^{-r^2/2R^2}$, R being the characteristic depth of the survey being studied.

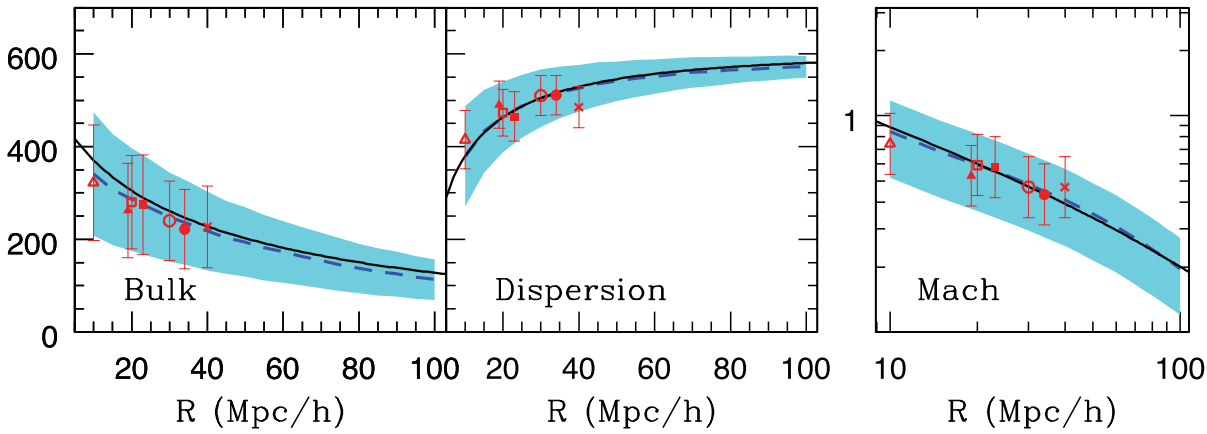

Figure 8. Similar to Fig. 7, but instead of showing linear theory predictions, we plot predictions based on the non-linear matter power spectrum for the LD cosmology estimated using PKANN.

A further simplification in the Mach analysis one can hope to achieve is to be able to predict $M(R)$ as a function of scale R without resorting to N-body simulations. Running high-resolution N-body simulations, even in the restricted parameter space around 7-yr *WMAP* (Komatsu et al. 2011) central parameters, is beyond present-day computing capabilities. It would be much easier and faster to explore the parameter space using a prescription for the matter power spectrum, and using equations (6) and (8) to predict the cosmic Mach number. So far, this has been possible by using linear theory. However, for linear theory results to be applicable, as mentioned in Section 1, one needs to correct for the non-linearities in the observed velocity field. Any residual non-linearity can still bias the Mach predictions.

In this section, we attempt to predict $M(R)$ using PKANN (Agarwal et al. 2012a) – a neural network interpolation scheme to predict the non-linear matter power spectrum up to $k \lesssim 0.9\,h\,\mathrm{Mpc}^{-1}$ between redshifts $z = 0$ and 2. Although PKANN accuracy worsens (starts underpredicting the non-linear spectrum for $k \gtrsim 0.9\,h\,\mathrm{Mpc}^{-1}$), we do not attempt to correct this by smoothing the velocity field over the relevant spatial scale. In Fig. 8, we replace linear theory predictions shown in Fig. 7 with the ones calculated using PKANN for the LD cosmology. PKANN (solid lines) gives a good match with the N-body results (dashed lines) on all scales, showing that PKANN can substitute numerical simulations for the purpose of calculating the Mach number given a set of cosmological parameters. Since PKANN predicts the power spectrum only up to $k \lesssim 1\,h\,\mathrm{Mpc}^{-1}$, the non-linear corrections are expected to be underestimated for smaller scales ($\sim 5\,h^{-1}$ Mpc) which get non-negligible contribution from higher k-modes. Although, we have shown PKANN's performance for only the LD cosmology, it is expected to perform satisfactorily for cosmologies around 7-yr *WMAP* central parameters for which PKANN has been specifically trained. See Agarwal et al. (2012a) for details on the parameter space of PKANN's validity.

8 MACH NUMBER ESTIMATES FROM REAL CATALOGUES

Ma et al. (2012) measured the Mach number for four peculiar velocity surveys (SBF, ENEAR, SNIa and SFI++f) and found that the ΛCDM model with 7-yr *WMAP* parameters is mildly consistent with the Mach number estimates for these four surveys at 3σ CL. However, as the authors mention in their work, their estimates are based on using a linear approximation for the power spectrum. Given the fact that at low redshifts structure formation has gone non-linear on small scales, it is necessary to consider non-linearities when making theoretical predictions. Comparing Figs 7 and 8 (middle panels), one can see that dispersion is significantly boosted by non-linearities, lowering the Mach predictions (third panels) by 1σ level.

Further, they work with top-hat window functions in their analysis. A top-hat filter assumes a volume-limited survey with a sharp edge in real space. However, the number density of objects sampled in a real survey typically falls at large distances. Real surveys thus have a narrower depth than what a top-hat would suggest. The sharp edge of a top-hat creates both ringing and extended tails in k-space. Since it is the small-scale modes that are most contaminated by non-linearities at low redshifts, a top-hat filter leads to aliasing of small-scale power on to larger scales. As such, a top-hat filter is a poor choice if one wants to isolate the contribution from small scales.

It is worth mentioning here that using a Gaussian window function $W^2(kR) = \mathrm{e}^{-K^2R^2}$ overdamps the high-k tails associated with a top-hat. The reason being that we only observe the line-of-sight component of the velocity field, whereas the equations presented in Section 2 are based on the full 3D velocity measurements. The line-of-sight component extends the tails of the survey window functions in k-space (see Grinstein et al. 1987; Kaiser 1988). This is the reason why in our analysis, we do not use $W^2(kR) = \mathrm{e}^{-K^2R^2}$; instead, we compute the ideal window functions using only the line-of-sight information (see equation 17). The extended tails of the ideal window functions can be seen in Fig. 6 and should be contrasted against $W^2(kR) = \mathrm{e}^{-K^2R^2}$.

Ma et al. (2012) estimated the characteristic depth of these surveys using $\sum w_n r_n / \sum w_n$, where $w_n = 1/(\sigma_n^2 + \sigma_*^2)$. Specifically, they found depths of 16.7, 30.5, 30.7 and 50.5 h^{-1} Mpc for the SBF, ENEAR, SNIa and SFI++f, respectively. However, from Fig. 6 and Table 3 (rows 1, 2, 4 and 5), we show that these surveys probe scales of $R \approx 10, 19, 23$ and $30\,h^{-1}$ Mpc, respectively. Using linear theory with top-hat filters, and neglecting the survey window functions while estimating the effective depths, makes the BF (and any derived) statistic highly complicated to interpret.

In Section 6.3, we used numerical simulations to study the Mach statistic for SBF, ENEAR, SFI++g, SNIa, SFI++f, DEEP and SC mocks. Now, we calculate the bulk, dispersion and the Mach numbers using the real catalogues themselves. The results are shown in Fig. 9 and summarized in Table 3, columns 7–9. We find that the Mach observations lie within the $\sim 1.5\sigma$ interval for a

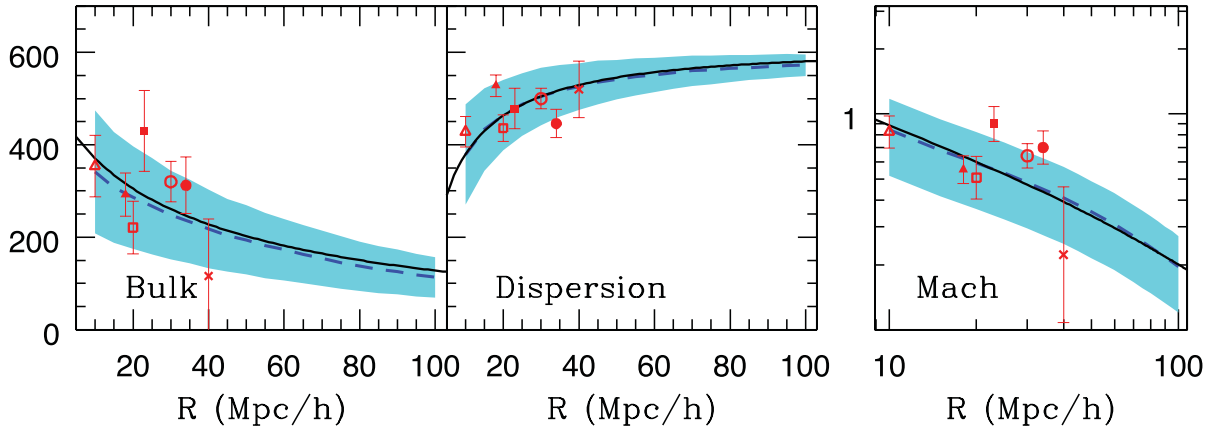

Figure 9. Similar to Fig. 8, but instead of the mocks, we plot the results for the real surveys. The error bars are calculated using the radial distance uncertainties.

ΛCDM universe with LD parameters. We attribute the high uncertainty in the Mach number for the SC catalogue to its poor sky coverage.

9 DISCUSSION AND CONCLUSIONS

The estimates of BF and dispersion on scale R are subject to observational errors stemming from the accuracy levels of distance indicators used and the survey geometry. Typically, the velocity power spectrum is smoothed using top-hat or Gaussian filters, with results depending on the exact smoothing procedure used. Often, BF results are quoted and inferences drawn about our cosmological model, without paying much attention to the survey window functions which are essential in determining the scales that contribute to quantities derived from peculiar velocities. A statistic such as the cosmic Mach number can be a useful tool to test theories of structure formation, provided the observational uncertainties are accounted for and the scale is properly determined.

In this paper, we studied the statistical distribution of the Mach number by extracting mock realizations of the real peculiar velocity catalogues from LD numerical simulations. We showed that the Mach number estimates from the real catalogues agree with the expectations for a ΛCDM universe at the $\sim 1.5\sigma$ level at the characteristic scales of the surveys. We checked if our Mach expectations derived from mock surveys were biased by the selection function effects: we extracted realizations with a Gaussian profile $f(r) \propto e^{-r^2/2R^2}$ and found no significant change to our Mach values for the mock surveys.

We compared results from numerical simulations to show that theoretical prediction of the Mach number based on linear theory of structure formation is inaccurate. Specifically, small-scale non-linearities increase velocity dispersion, thereby lowering the Mach predictions by about 1σ for a ΛCDM universe with *WMAP*-type cosmology. We presented an alternative method to study the cosmic Mach number – by using a prescription for the non-linear matter power spectrum, instead of running time-consuming and computationally intensive numerical simulations. Non-linear power spectrum interpolators like PKANN offer tremendous leverage over numerical simulations, by being able to explore the parameter space quickly. The role of such interpolating schemes in the study of quantities derived from peculiar velocities needs further investigation. Also, in the future we plan to employ a MV-like formalism to study this statistic, reduce the non-linear signal to below the statistical errors and thus create a truly linear Mach number statistic that can be used to directly compare results from disparate surveys as a function of the volume chosen and probed.

ACKNOWLEDGEMENTS

We are grateful to Róman Scoccimarro and the LasDamas collaboration for providing us with the simulations. We thank Richard Watkins and Maciej Bilicki for their thoughtful comments and discussion. This work was supported in part by the National Science Foundation through TeraGrid resources provided by the NCSA.

REFERENCES

Agarwal S., Abdalla F. B., Feldman H. A., Lahav O., Thomas S. A., 2012a, MNRAS, 424, 1409
Agarwal S., Feldman H. A., Watkins R., 2012b, MNRAS, 424, 2667
Bahcall N. A., Oh S. P., 1996, ApJ, 462, L49
Bahcall N. A., Gramann M., Cen R., 1994, ApJ, 436, 23
Bernardi M., Alonso M. V., da Costa L. N., Willmer C. N. A., Wegner G., Pellegrini P. S., Rité C., Maia M. A. G., 2002, AJ, 123, 2990
Colless M., Saglia R. P., Burstein D., Davies R. L., McMahan R. K., Wegner G., 2001, MNRAS, 321, 277
da Costa L. N., Bernardi M., Alonso M. V., Wegner G., Willmer C. N. A., Pellegrini P. S., Rité C., Maia M. A. G., 2000, AJ, 120, 95
Dale D. A., Giovanelli R., Haynes M. P., Campusano L. E., Hardy E., 1999, AJ, 118, 1489
Davis M., Efstathiou G., Frenk C. S., White S. D. M., 1985, ApJ, 292, 371
Feldman H. A., Watkins R., 1994, ApJ, 430, L17
Feldman H. A., Watkins R., Hudson M. J., 2010, MNRAS, 407, 2328
Gardner J. P., Connolly A., McBride C., 2007, in Shaw R. A., Hill F., Bell D. J., eds, ASP Conf. Ser. Vol. 376, Astronomical Data Analysis Software and Systems XVI. Astron. Soc. Pac., San Francisco, p. 69
Giovanelli R., Haynes M. P., Salzer J. J., Wegner G., da Costa L. N., Freudling W., 1998, AJ, 116, 2632
Grinstein B., Politzer H. D., Rey S.-J., Wise M. B., 1987, ApJ, 314, 431
Hudson M. J., Smith R. J., Lucey J. R., Schlegel D. J., Davies R. L., 1999, ApJ, 512, L79
Hudson M. J., Colless M., Dressler A., Giovanelli R., 2000, in Courteau S., Willick J., eds, ASP Conf. Ser. Vol. 201, Cosmic Flows Workshop. Astron. Soc. Pac., San Francisco, p. 159
Hudson M. J., Smith R. J., Lucey J. R., Branchini E., 2004, MNRAS, 352, 61
Kaiser N., 1988, MNRAS, 231, 149
Komatsu E. et al., 2011, ApJS, 192, 18
Linder E. V., 2005, Phys. Rev. D, 72, 043529
Ma Y.-Z., Ostriker J. P., Zhao G.-B., 2012, J. Cosmol. Astropart. Phys., 6, 26

Masters K. L., Springob C. M., Haynes M. P., Giovanelli R., 2006, ApJ, 653, 861
McBride C., Berlind A., Scoccimarro R., Wechsler R., Busha M., Gardner J., van den Bosch F., 2009, BAAS, 41, 425.06
Nishimichi T. et al., 2009, PASJ, 61, 321
Ostriker J. P., Suto Y., 1990, ApJ, 348, 378
Saito S., Takada M., Taruya A., 2008, Phys. Rev. Lett., 100, 191301
Saito S., Takada M., Taruya A., 2009, Phys. Rev. D, 80, 083528
Sarkar D., Feldman H. A., Watkins R., 2007, MNRAS, 375, 691
Smith R. E. et al., 2003, MNRAS, 341, 1311
Springob C. M., Masters K. L., Haynes M. P., Giovanelli R., Marinoni C., 2007, ApJS, 172, 599
Springob C. M., Masters K. L., Haynes M. P., Giovanelli R., Marinoni C., 2009, ApJS, 182, 474
Strauss M. A., Cen R., Ostriker J. P., 1993, ApJ, 408, 389
Suto Y., Cen R., Ostriker J. P., 1992, ApJ, 395, 1
Tonry J. L., Dressler A., Blakeslee J. P., Ajhar E. A., Fletcher A. B., Luppino G. A., Metzger M. R., Moore C. B., 2001, ApJ, 546, 681
Tonry J. L. et al., 2003, ApJ, 594, 1
Watkins R., 1997, MNRAS, 292, L59
Watkins R., Feldman H. A., 1995, ApJ, 453, L73
Watkins R., Feldman H. A., 2007, MNRAS, 379, 343
Watkins R., Feldman H. A., Hudson M. J., 2009, MNRAS, 392, 743
Wegner G. et al., 2003, AJ, 126, 2268
Willick J. A., 1999, ApJ, 522, 647

This paper has been typeset from a TEX/LATEX file prepared by the author.